A TWO-PARAMETER MODEL FOR THE INFRARED/SUBMILLIMETER/RADIO SPECTRAL ENERGY DISTRIBUTIONS OF GALAXIES AND AGN

Daniel A. Dale[1], George Helou[2], Georgios E. Magdis[3], Lee Armus[4], Tanio Díaz-Santos[4], and Yong Shi[5]

ABSTRACT

A two-parameter semi-empirical model is presented for the spectral energy distributions of galaxies with contributions to their infrared-submillimeter-radio emission from both star formation and accretion disk-powered activity. This model builds upon a previous one-parameter family of models for star-forming galaxies, and includes an update to the mid-infrared emission using an average template obtained from *Spitzer Space Telescope* observations of normal galaxies. Star-forming/AGN diagnostics based on PAH equivalent widths and broadband infrared colors are presented, and example mid-infrared AGN fractional contributions are estimated from model fits to the GOALS sample of nearby LIRGS and the 5MUSES sample of 24 μm-selected sources at redshifts $0 \lesssim z \lesssim 2$.

Subject headings: ISM: general — galaxies: ISM — infrared: ISM

1. Introduction

There have been many recent developments in modelling galaxy infrared spectral energy distributions. Some of these models are quite sophisticated, and when fitted to a galaxy's observed spectrum, their various parameters can yield insight into the physical characteristics of the system (e.g., Silva et al. 1998; Popescu et al. 2000; Gordon et al. 2001; Siebenmorgen

---

[1]Department of Physics & Astronomy, University of Wyoming, Laramie, WY 82071, USA; ddale@uwyo.edu

[2]Infrared Processing and Analysis Center, California Institute of Technology, Pasadena, CA 91125, USA

[3]Department of Physics, University of Oxford, Keble Road, Oxford OX1 3RH, UK

[4]Spitzer Science Center, California Institute of Technology, Pasadena, CA 91125, USA

[5]School of Astronomy and Space Science, Nanjing University, Nanjing, 210093, China

& Krügel 2007; Draine & Li 2007; da Cunha et al. 2008; Galliano et al. 2008; Groves et al. 2008; Hermelo et al. 2013). Such models are often referred to as "grids" to reflect their multi-dimensional nature. At the other extreme of infrared galaxy spectral models are one-dimensional "templates", typically a suite of synthetic or empirical spectra that essentially rely on a single parameter to characterize a galaxy's infrared spectral shape. For example, Chary & Elbaz (2001) and Rieke et al. (2009) provide template spectra sequenced according to their bolometric infrared luminosity $L_{\rm TIR}$. Similarly, Dale & Helou (2002) use a "single parameter family" (denoted by their $\alpha_{\rm SF}$) to coherently govern changes across their templates in polycyclic aromatic hydrocarbon (PAH) emission, the peak wavelength of the broad far-infrared bump, and the far-infrared/submillimeter dust emissivity. The work presented in Spoon et al. (2007) represents an example of a spectral set that is intermediate in complexity between grids and templates, whereby the strength of the 9.7 μm silicate absorption and the 6.2 μm PAH equivalent width form the basis of their two-dimensional system for describing mid-infrared spectra. In deciding which set(s) of models to adopt, the end users ultimately must balance their need for sophisticated interpretation with ease of use. This choice depends on a project's science goals and the richness of the observational dataset.

Complicating this choice is the additional issue of infrared emission from active galactic nuclei (AGN); for many galaxies, a full accounting of their infrared energy budget must include dust for which the heating can be traced to accretion disk-powered luminosity around supermassive black holes, especially for more luminous systems (e.g., Del Moro et al. 2013; Shi et al. 2013; Kirkpatrick et al. 2013). This concern is especially true for interpreting galaxies at higher redshifts ($z \sim 2-3$), where the fraction of quasars and strong AGN galaxies is higher than at the present epoch (Fan et al. 2001). For example, work by Goto et al. (2010) and Fu et al. (2010) suggest that a significant portion of the evolution with redshift in the cosmic infrared luminosity function can be attributed to the increased fraction of AGN in the overall galaxy population at higher redshifts. Thus, ideally each set of infrared galaxy spectral energy distribution models would have a convenient methodology for consideration of AGN contributions. Some models do incorporate dust emission from both AGN and star formation (Siebenmorgen & Krügel 2007; Rieke et al. 2009; Berta et al. 2013), but most do not. However, the clear challenge in this arena is the paucity of robust multi-wavelength AGN databases, particularly databases where it is clear that the majority of the infrared emission does indeed come from the AGN and not from star-forming regions. Fortunately, recent progress in robust panchromatic AGN datasets present opportunities to remedy this limitation in galaxy spectral modeling (e.g., Richards et al. 2006; Shang et al. 2011; Mullaney et al. 2011).

We report here efforts to update the infrared/submillimeter/radio spectral energy distribution models from Dale & Helou (2002) in two important ways. First, we update the mid-infrared portion of these star-forming models, which was originally based on ISOPHOT data from the Infrared Space Observatory, using results from the *Spitzer Space Telescope*. The main improvement resulting from this modification is the inclusion of the prominent 17 μm PAH complex, which can produce up to 10% of the total PAH emission. Second, we add another spectral component that represents emission from AGN; the models in Dale & Helou (2002) were purely for star-forming systems. For this AGN component, the panchromatic database of radio-quiet quasars from Shang et al. (2011) is employed. A radio-quiet quasar template is adopted (versus a radio-loud template) since in the local universe radio-quiet quasars comprise approximately 90% of the quasar population (Ivezić et al. 2001; Jiang et al. 2007). We test this new model using data from the *Spitzer Space Telescope* and *Herschel Space Observatory* and the 5MUSES (Wu et al. 2010) and GOALS (Armus et al. 2009) surveys, surveys for which AGN percentages have been independently estimated from infrared data (Petric et al. 2011; Wu et al. 2011). In the process, we show these models are applicable to the Luminous Infrared Galaxy (LIRG) and UltraLuminous Infrared Galaxy (ULIRG) regimes ($L_{\rm TIR} > 10^{11} L_\odot$ and $L_{\rm TIR} > 10^{12} L_\odot$, respectively); the models were originally developed using only "normal" star-forming galaxies ($L_{\rm TIR} \lesssim 10^{10} L_\odot$).

In Section 2 we review the two galaxy samples against which the updated models are tested. Section 3 describes how the templates are updated using recent databases on AGN and star-forming galaxies, and Section 4 presents the results from this work. The final section summarizes our findings.

2. Samples for Testing the Model

Two galaxy surveys are used to check the utility of the spectral energy distribution models described below (see Figure 1). The first survey is the Five mJy Unbiased Spitzer Extragalactic Survey ("5MUSES"; Wu et al. 2010), a 24 μm-selected sample of 330 galaxies spanning redshifts $0 \lesssim z \lesssim 2$ for which *Spitzer* IRS low-resolution spectra (5–35 μm) were obtained (high resolution IRS spectroscopy was also obtained for a subset of the sample). In addition to the extant *Spitzer* IRAC and MIPS photometry for 5MUSES that is available from the SWIRE (Lonsdale et al. 2003) and First Look Surveys (Fadda et al. 2006), we also have new Herschel 250, 350, and 500 μm SPIRE fluxes (Magdis et al. 2013). These Herschel data were taken as part of the HerMES project (Oliver et al. 2010), and probe to a 50% source recovery limit of 12–30 mJy. Overall, secure SPIRE photometry for all three passbands exists for 74 5MUSES targets.

The second comparative sample stems from the Great Observatories All-Sky LIRG Survey ("GOALS"; Armus et al. 2009). This survey includes deep *Spitzer* IRS spectroscopy for 202 nearby LIRGs and ULIRGs covering a redshift range of $0 \lesssim z \lesssim 0.09$. Broadband infrared data from *Spitzer* IRAC 3.6/4.5/5.8/8.0 μm and *Spitzer* MIPS 24/70/160 μm also exist for GOALS, and we utilize the published photometry for a subset of 64 sources (U et al. 2012). Using the mid-infrared continuum spectral diagnostics developed in Laurent et al. (2000), the typical AGN fractional contribution to the mid-infrared energy budget in GOALS sources is 15% (Petric et al. 2011).

3. The Updated Spectral Energy Distribution Models

In the original construction of these templates (Dale et al. 2001; Dale & Helou 2002), a series of "local" spectral energy distributions were created to represent the emission from dust exposed to a wide range of heating intensities $0.3 \leq U \leq 10^5$ where $U = 1$ corresponds to the local interstellar radiation field in the Solar Neighborhood. A power-law combination of these local curves can effectively mimic the spatially-integrated ("global") dust emission, i.e.,

$$dM_{\rm d} \propto U^{-\alpha_{\rm SF}} dU, \tag{1}$$

where $M_{\rm d}$ is the dust mass heated by a radiation field at intensity U and the exponent $\alpha_{\rm SF}$ represents the relative contributions of the different local spectral energy distributions.

These templates were built on the framework of Désert, Boulanger, & Puget (1990) and are comprised of emission from stochastically-heated PAHs, emission from semi-stochastically heated very small grains, and thermal emission from large dust grains. Various modifications based on observations of star-forming galaxies were made by Dale and collaborators to the Désert, Boulanger, & Puget (1990) framework, including the insertion of an empirical PAH spectrum, the incorporation of a wavelength-dependent far-infrared/sub-millimeter dust emissivity, and the extension of their modeling to radiation fields $U > 10^3$.

The average 2.5–11.5 μm mid-infrared spectrum of Lu et al. (2003) was used to replace the PAH spectrum of Désert, Boulanger, & Puget (1990). This spectral energy distribution was derived from the average of 40 normal star-forming disk galaxies from the *Infrared Space Observatory* Key Project on Normal Galaxies (Dale et al. 2000). Though this *ISO* spectrum represented a step forward in infrared spectral energy distribution modeling at the time, a description here of some of its features and limitations is warranted. Those data were taken with the ISOPHOT instrument aboard *ISO*, an instrument which had a $24'' \times 24''$ field of view, resulting in relatively large ~ 4 kpc sizescales over which the galaxies were sampled; the average ISOPHOT spectra undoubtedly contained contributions from a wide range of environments (e.g., H II regions; photo-dissociation regions, molecular clouds, etc.), a feature that may not be desirable for certain modeling applications. A significant limitation to the

Lu et al. (2003) spectrum is that it is restricted to wavelengths 2.5 μm $\leq \lambda \leq$ 11.5 μm with a gap in coverage between 4.8 and 5.8 μm. The wavelength gap was bridged with a simple linear interpolation of the average spectrum. Finally, the 11.5 μm cut-off to the red end of the ISOPHOT spectrum unfortunately resulted in a truncated tracing of the 11.3 μm PAH feature and the omission of the 12.7 μm PAH emission feature and those at any longer wavelengths. This latter limitation was partly remedied in Dale et al. (2001) by a schematic extension to 15 μm that was guided by ISOCAM CVF observations.

3.1. Modifications to the Star-Forming Templates

For the updated mid-infrared spectrum we adopt the 5–34 μm "pure" star-forming curve from Spoon et al. (2007) (their spectrum '1C'), who utilized the *Spitzer* archives to analyze a sequence of mid-infrared spectral shapes among AGN, ULIRGs, and star-forming galaxies. Important benefits to updating the mid-infrared with *Spitzer* data are the inclusion of prominent fine-structure lines (e.g., [Ne III]15.6 μm, [S III]18.7 μm, and [S III]33.5 μm) and the 17 μm PAH complex, the latter of which accounts for up to 10% of the total PAH emission in normal star-forming galaxies (see Figure 2 of this work and Table 7 of Smith et al. 2007). As was done in Dale et al. (2001), we scale the empirical mid-infrared spectrum to the amplitude of the Désert, Boulanger, & Puget (1990) PAH templates via integrating over the 12 μm IRAS filter. The shape of the mid-infrared continuum beyond 15 μm was also fixed to that of the Désert, Boulanger, & Puget (1990) PAH templates. Besides these modifications to the mid-infrared spectrum, the star-forming templates are otherwise unchanged. We continue to utilize a single-parameter family (i.e., α_{SF}) to describe the full range of PAH/very small grain/large grain and overall spectral shapes for normal star-forming galaxies. Moreover, it should be noted that we continue to assume optically thin infrared emission, and thus do not include in our model any absorption features such as the 9.7 μm silicate trough found in many ULIRGs (e.g., Armus et al. 2007). While this simplification will fail to appropriately characterize all the nuances in mid-infrared spectra for samples specifically selected to be infrared-luminous (e.g., GOALS; Stierwalt et al. 2013), there are very few deeply obscured systems in infrared flux-limited surveys like 5MUSES (Wu et al. 2010).

3.2. Addition of an AGN Template

While the star-forming templates themselves from Dale & Helou (2002) are only slightly modified, we introduce here a fundamental addition to the templates by incorporating a second parameter, one that accounts for accretion disk-powered infrared luminosity.

Until recently, the state-of-the-art in panchromatic quasar spectral energy distributions was still the pioneering work of Elvis et al. (1994), who studied 47 non-blazar quasars (29 radio-quiet and 18 radio-loud) from the radio through 10 keV X-rays. However, the recent influx of large multi-wavelength databases has allowed for more complete reconstructions of quasar energy distributions. In 2011, Shang and collaborators updated the Elvis et al. (1994) work using data from 85 non-blazar quasars (27 radio-quiet and 58 radio-loud). The data involved in their analysis include X-ray, far- and near-ultraviolet, optical, near-, mid-, and far-infrared, and radio spectroscopy and/or photometry. We adopt here the radio-quiet and not the radio-loud spectrum of Shang et al. (2011) since in the local universe it is estimated that ∼90% of the quasars are radio-quiet (Ivezić et al. 2001; Jiang et al. 2007). However, one important modification has been incorporated. As a precaution to ensure that any star formation-related contributions from the host galaxy are limited, the emission beyond ∼120 μm is forced to drop like a blackbody ($\nu f_\nu \propto \lambda^{-4}$; see also Figure 3 of Shi et al. 2013).

Figure 2 displays this (slightly modified) median radio-quiet quasar spectral energy distribution of Shang et al. (2011) in addition to a suite of normal star-forming galaxy curves spanning a range in $\alpha_{\rm SF}$. Several features are evident in the median quasar spectrum, including the broad silicate emission features near 10 and 18 μm and the [O IV] 25.9 μm fine structure line that are seen in many AGN (Hao et al. 2005; Armus et al. 2007). To simulate the spectral appearance of a source for which the emission has contributions from both an AGN and normal star formation, we employ linear mixing over the 5–20 μm wavelength range. For this work we have developed mixed combinations for 5–20 μm AGN fractions running from 0% to 100%, spaced at 5% intervals.[1] Figure 3 shows how the resulting infrared–radio spectral energy distributions appear for an equal contribution from AGN and star-forming emission.

4. Results

4.1. Model Color Distributions

To date most efforts to disentangle infrared emission from AGN and star formation have focused on utilizing mid-infrared continuum datasets (e.g., Laurent et al. 2000; Murphy et al. 2009; Mullaney et al. 2011; Wu et al. 2011) or a combination of the mid-infrared continuum plus mid-infrared fine-structure lines (e.g., Genzel et al. 1998; Peeters et al. 2004;

[1] Available at physics.uwyo.edu/∼ddale/research/seds/seds.html

Armus et al. 2007; Dale et al. 2009). A common complementary technique for identifying AGN contributions, especially useful when mid-infrared spectral data are unavailable, involves combinations of flux ratios that utilize data from three or four broadband filters (e.g., Lacy et al. 2004; Stern et al. 2005; Yan et al. 2013; Kirkpatrick et al. 2013; Mendez et al. 2013). Figure 4 shows how the various combinations of the star-forming and AGN templates appear in two different infrared color-color diagrams (assuming rest wavelengths). Using such continuum diagnostics, one can estimate both the AGN fractional contribution as well as the characteristics of the star-forming portion of the galaxy, e.g., dust temperature. The colors for local actively star-forming galaxies (filled squares) shown in Figure 4 come from Siebenmorgen & Krügel (2007), the colors for normal star-forming galaxies (open circles) are from Dale et al. (2012), and the colors for the local AGN M 87 (filled triangle) are from NED; the $f_\nu(70\mu\text{m})/f_\nu(500\mu\text{m})$ color for M 87 falls below the displayed range since the 500 μm flux is overwhelmed by synchrotron radiation (Baes et al. 2010). Note that our color-color analysis does not to extend to wavelengths shorter than 8 μm and thus cannot be directly compared to *Spitzer* IRAC color-color analyses (e.g., Lacy et al. 2004; Stern et al. 2005). This restriction is by design: the Spoon et al. (2007) star-forming template begins at 5 μm, a feature which conveniently minimizes complications arising from stellar emission.

4.2. PAH Equivalent Width Distributions

The strengths of various PAH features have been widely used to diagnose the main power source of a galaxy (e.g., Genzel et al. 1998; Laurent et al. 2000; Armus et al. 2007; Smith et al. 2007; Spoon et al. 2007; Dale et al. 2009; Hernán-Caballero et al. 2009; Diamond-Stanic & Rieke 2010; Wu et al. 2010; Shang et al. 2011). These studies suggest that $EW(\text{PAH}6.2\mu\text{m}) \approx 0.2$ μm is an approximate delineation between sources predominantly powered by AGN and those mostly powered by star formation. Figure 5 shows how the PAH(6.2 μm) equivalent widths for our models depend on far-infrared color. The different curves show the trends for a variety of AGN fractions; the 6.2 μm equivalent width for the Spoon et al. (2007) pure star-forming curve used here is ~ 0.5 μm. As can be seen from the figure, larger AGN fractions correspond to lower equivalent width, attributable to the fact that the adopted AGN template is essentially devoid of PAH emission features. Moreover, each trend of connected points in Figure 5 dips to lower equivalent widths at warmer far-infrared colors, a feature that complicates using the 6.2 μm equivalent width as a pure AGN/star-forming diagnostic. This effect of diminished PAH strength (equivalent width) as a function of star formation activity level is weakly built in to the star-forming models (see Figure 6 of Dale et al. 2001), echoing the results of diminished PAH emission for regions permeated by hard radiation fields (Madden et al. 2006). The effect is accentuated when an AGN continuum is added to the mid-infrared. In addition, even "pure" star-forming galaxies exhibit a significant dispersion in the equivalent width of PAH features (e.g., 0.2 dex at 6.2 μm; Wu et al. 2010), a dispersion that these simple models do not incorporate. However, in agreement with the references listed above, this plot shows that $EW(\mathrm{PAH6.2}\mu\mathrm{m}) \approx 0.2 - 0.3$ μm could roughly be used as a demarcation between sources powered by SF and AGN activity.

4.3. Spectral Energy Distribution Fits

Figure 6 shows the best fits of the AGN/star-forming curves to the subset of 5MUSES sources that have *Herschel* SPIRE data available. The fits are carried out via a χ^2 minimization using infrared colors:

$$\chi^2 = \sum_{i,j<i} \frac{\left(\log \frac{f_{\nu,i}^{\mathrm{obs}}}{f_{\nu,j}^{\mathrm{obs}}} - \log \frac{f_{\nu,i}^{\mathrm{model}}}{f_{\nu,j}^{\mathrm{model}}}\right)^2}{(\sigma_{i,j}^{\mathrm{obs}})^2}, \tag{2}$$

where $\log \frac{f_{\nu,i}^{\mathrm{obs}}}{f_{\nu,j}^{\mathrm{obs}}}$ and $\log \frac{f_{\nu,i}^{\mathrm{model}}}{f_{\nu,j}^{\mathrm{model}}}$ are respectively the observed and model colors involving bandpasses i and j, and σ_b^{obs} is the uncertainty in the observed color. The model colors are obtained after convolving the model with the appropriate filter bandpasses. The colors used in the fit involve all possible combinations of the *Spitzer* IRAC 5.8/8.0 μm, *Spitzer* MIPS 24/70/160 μm, and *Herschel* SPIRE 250/350/500 μm flux densities, except for the minority of higher redshift targets for which the central wavelengths of certain shorter-wavelength filter bandpasses correspond to rest wavelengths shorter than 5 μm. For example, the 5.8 and 8.0 μm data are not used in the fit for lh38 at $z = 1.814$ and the 5.8, 8.0, and 24 μm data are not used in the fit for fls25 at $z = 4.270$.

The values of α_{SF} and the AGN percentage found in each panel of Figure 6 correspond to the median value obtained after carrying out 1000 Monte Carlo simulations of each fit. For each Monte Carlo simulation, a random (Gaussian deviate) flux offset, scaled according to the measured uncertainty, was added to each flux.

4.4. Comparison with Other AGN Fractional Estimates

The mid-infrared AGN fractions for galaxies from the 5MUSES survey are provided within the subpanels of Figure 6. Sixty-eight percent of the subsample has mid-infrared AGN fractions less than 50%, and the mid-infrared AGN fraction unsurprisingly scales strongly with luminosity (see § 4.5). These 3.6–500 μm SED-fitting-based mid-infrared AGN fractional estimates for both the 5MUSES survey and the GOALS survey can be compared to estimates found in the literature (see Figure 7). The 5MUSES mid-infrared AGN fractions are compared to those from Wu et al. (2011), who utilize the 5–35 μm continuum data and various templates of AGN and star-forming systems. The GOALS mid-infrared AGN fractions are compared to those from Petric et al. (2011), who employ the mid-infrared spectroscopic diagnostic of Laurent et al. (2000) which conceptually relates the slope of the 5–15 μm continuum to the equivalent width of the 6.2 μm PAH feature. The mean differences between our mid-infrared AGN percentages and those from the literature, expressed in terms of the uncertainties, are relatively close to zero—$0.5\epsilon_{\rm tot}$ for 5MUSES and $0.1\epsilon_{\rm tot}$ for GOALS—and the standard deviations in the differences are $0.8\epsilon_{\rm tot}$ (5MUSES) and $0.9\epsilon_{\rm tot}$ (GOALS). The uncertainty $\epsilon_{\rm tot}$ is a sum in quadrature of the standard deviations in the Monte Carlo simulations decribed in § 4.3, a 25% uncertainty assigned to the literature fractional values, and a flat 20% to account for uncertainties intrinsic to the literature methodology.

For the comparison involving GOALS, these differences in the mid-infrared AGN fractional estimates are dispersed at a level about what would be expected for a normal distribution, for which the expectation is of course a null average difference and a dispersion of $1.0\epsilon_{\rm tot}$. A (nonparametric) Spearman rank correlation test yields a correlation coefficient of only 0.31 and thus, for the 40 targets for which reliable mid-infrared AGN fractions are available from both Petric et al. (2011) and this work, there is a $\sim$3% probability that this weak correlation occurred purely through chance. In short, the correspondence between the two techniques for the GOALS sample is weak. The comparison is stronger involving the 5MUSES sample: the Spearman correlation coefficient is 0.68 and thus there is less than a 1% probability that the correlation occurred purely through chance.

4.5. Total Infrared Estimators and AGN Fraction

Simple prescriptions for estimating the total luminosity over 5–1100 μm[2] can be obtained from linear combinations of different broadband fluxes, e.g.,

$$L_{\rm TIR} = \eta_1 \nu L_\nu(25\mu{\rm m}) + \eta_2 \nu L_\nu(60\mu{\rm m}) + \eta_3 \nu L_\nu(100\mu{\rm m}) \qquad ({\rm IRAS-based}), \tag{3}$$

$$L_{\rm TIR} = \zeta_1 \nu L_\nu(24\mu{\rm m}) + \zeta_2 \nu L_\nu(70\mu{\rm m}) + \zeta_3 \nu L_\nu(160\mu{\rm m}) \qquad ({\rm Spitzer-based}), \tag{4}$$

[2]The TIR wavelength range defined here is slightly different from the 3-1100 μm wavelength range presented in Dale & Helou (2002) in order to minimize any influence from stellar emission in observed spectral energy distributions.

$$L_{\rm TIR} = \xi_0 \nu L_\nu(8\mu{\rm m}) + \xi_1 \nu L_\nu(24\mu{\rm m}) + \xi_2 \nu L_\nu(70\mu{\rm m}) + \xi_3 \nu L_\nu(160\mu{\rm m}) \ \ ({\rm Spitzer-based}) \quad (5)$$

where the coefficients are functions of the AGN fractional contribution to the 5–20 μm mid-infrared luminosity (for other recent formulations see also Boquien et al. 2010; Elbaz et al. 2011; Galametz et al. 2013). The coefficients are derived from a singular value decomposition solution to an overdetermined set of linear equations involving the individual broadband luminosities as well as the total infrared luminosity (*TIR*). Table 1 gives the various coefficients for a range of mid-infrared AGN fractions and assuming rest-frame quantities. For the pure star-forming sequence (i.e., the top row of 0% AGN), the coefficients are similar to those already published in Dale & Helou (2002).

The maximum error listed in Table 1 indicates the largest deviation of the *TIR* approximation, with the respect to the actual *TIR*, observed for the sequence of star-forming models parameterized by $\alpha_{\rm SF}$. The noticeably smaller maximum errors of the 24/70/160 μm combination implies that this filter triplet does a better job of sampling the full infrared profile than the more wavelength-limited IRAS 25/60/100 μm combination; likewise, using the four 8/24/70/160 μm *Spitzer* fluxes better captures the full range of model variations than using just the three *Spitzer*/MIPS fluxes. The 70 and 160 μm coefficients in Equations 4 and 5 have formally been derived assuming *Spitzer*/MIPS bandpasses, but similar values are obtained for *Herschel*/PACS 70 and 160 μm bandpasses.

Figure 8 shows how the 5MUSES sample is biased toward AGN at higher infrared luminosities. Above a luminosity of $L({\rm TIR}) \sim 5 \cdot 10^{11}\ L_\odot$, nearly all 5MUSES sources with *Spitzer* and *Herschel* photometry are estimated to be dominated by AGN. For reference, a similar evolution in AGN fraction with luminosity is seen for infrared-selected AKARI sources (see Figure 5 in Goto et al. 2011). The U et al. (2012) subset of the GOALS sample covers a much more limited range in luminosity and hence any trend is difficult to ascertain.

5. Summary

A two-parameter family of infrared/submillimeter/radio spectral energy distribution models is presented. The first parameter governs the variety of long-wavelength spectral shapes observed for star-forming galaxies, whereas the second parameter quantifies the fractional contribution of AGN mid-infrared emission. The star-forming models are based on those presented in Dale & Helou (2002) and incorporate updates at mid-infrared wavelengths using *Spitzer* spectral data. The AGN parameterization relies on the recent progress in generating panchromatic quasar databases. The particular spectrum adopted for this modeling effort is the median spectrum derived from a sample of 27 non-blazar radio-quiet quasars (Shang et al. 2011). Because only two parameters are utilized, the fine-scale interpretive power of these models is necessarily limited, and they do not capture the full range of observed spectra. For example, optically thin emission is assumed and thus the models do not have the flexibility to account for the deep 9.7 μm silicate aborption that can be evident in the spectra of many ULIRGs and quasars for which the accretion disks are viewed edge-on. Neither do the models capture the full range of observed star-forming infrared spectra (e.g., SBS 0335-052 and NGC 1377 Houck et al. 2004; Roussel et al. 2006). However, the models do a remarkable job in capturing the broad features seen in the infrared/submillimeter continuua of multiple galaxy samples that span a large range in redshift, AGN activity, and infrared luminosity. Moreover, our estimates of the AGN fractional contributions to the mid-infrared luminosity are consistent with those previously published for these samples. Perhaps the most interesting feature to these models is their ability to effectively quantify the AGN fraction based solely on broadband infrared photometry; previous infrared-based efforts tend to require having spectroscopy over a substantial range of mid-infrared wavelengths (e.g., Murphy et al. 2009; Wu et al. 2011). Future efforts in developing "minimal" galaxy spectral models, ie., those that rely on a minimum number of parameters, should focus on capturing the rich diversity of mid-infrared spectral slopes, PAH equivalent widths, and silicate absorptions evident in galaxy and AGN spectra.

Support for this work, part of the *Spitzer Space Telescope* Legacy Science Program 40539, was provided by NASA and issued by the Jet Propulsion Laboratory, California Institute of Technology under NASA contract 1407. *Herschel* is an ESA space observatory with science instruments provided by European-led Principal Investigator consortia and with important participation from NASA. This research has made use of the NASA/IPAC Infrared Science Archive, which is operated by the Jet Propulsion Laboratory, California Institute of Technology, under contract with NASA. We gratefully acknowledge NASA's support for construction, operation, and science analysis for the GALEX mission, developed in cooperation with the Centre National d'Etudes Spatiales of France and the Korean Ministry of Science and Technology. Funding for the Sloan Digital Sky Survey and SDSS-II has been provided by the Alfred P. Sloan Foundation, the Participating Institutions, the NSF, the U.S. Department of Energy, NASA, the Japanese Monbukagakusho, the Max Planck Society, and the Higher Education Funding Council for England. This publication makes use of data products from the Two Micron All Sky Survey, which is a joint project of the University of Massachusetts and the Infrared Processing and Analysis Center/California Institute of Technology, funded by the National Aeronautics and Space Administration and the National Science Foundation.

REFERENCES

Armus, L. et al. 2007, ApJ, 656, 148

Armus, L. et al. 2009, PASP, 121, 559

Babbedge, T.S.R. et al. 2006, MNRAS, 370, 1159

Baes, M. et al. 2010, A&A, 518, 53

Berta, S. et al. 2013, A&A, 551, 100

Boquien, M. et al. 2010, ApJ, 713, 626

Chary, R. & Elbaz, D. 2001, ApJ, 556, 562

da Cunha, E., Charlot, S., & Elbaz, D. 2008, MNRAS, 388, 1595

Dale, D.A. et al. 2000, AJ, 120, 583

Dale, D.A., Helou, G., Contursi, A., Silbermann, N.A., & Kolhatkar, S. 2001, ApJ, 549, 215

Dale, D.A. & Helou 2002, ApJ, 576, 159

Dale, D.A., et al. 2009, ApJ, 693, 1821

Dale, D.A., et al. 2012, ApJ, 745, 95

Del Moro, A. et al. 2012, A&A, 549, 59

Désert, F.X, Boulanger, F. & Puget, J.L. 1990, A&A, 237, 215

Diamond-Stanic, A.M. & Rieke, G.H. 2010, ApJ, 724, 140

Draine, B.T. & Li, A. 2007, ApJ, 657, 810

Elbaz, D., et al. 2011, A&A, 533, A119

Elvis, M., Wilkes, B.J., McDowell, J.C., Green, R.F., Bechtold, J., Willner, S.P., Oey, M.S., Polomski, E., & Cutri, R. 1994 ApJS, 95, 1

Fadda, D. et al. 2006, AJ, 131, 2859

Fan, X. et al. 2001, ApJ, 121, 54

Fu, H. et al. 2010, ApJ, 722, 653

Galametz, M. et al. 2013, MNRAS, 431, 1956

Galliano, F., Dwek, E., and Chanial, P. 2008, ApJ, 672, 214

Genzel, R. 1998, ApJ, 498, 579

Gordon, K.D., Misselt, K.A., Witt, A.N., & Clayton, G.C. 2001, ApJ, 551, 269

Goto, T. et al. 2010, A&A, 514, 6

Goto, T. et al. 2011, MNRAS, 414, 1903

Groves, B., Dopita, M.A., Sutherland, R.S., Kewley, L.J., Fischera, J., Leitherer, C., Brandl, B., & van Breugel, W. 2008, ApJS, 176, 438

Hao, L. et al. 2005, ApJ, 625, L75

Hermelo, I., Lisenfeld, U., Relaño, M., Tuffs, R.J., Popescu, C.C., & Groves, B. 2013, A&A, 549, 70

Hernán-Caballero, A. et al. 2009, MNRAS, 395, 1695

Houck, J.R. et al. 2004, ApJS, 154, 211

Ivezić, Z. et al. 2001, AJ, 124, 2364

Jiang, L., Fan, X., Ivezić, Z., Richards, G.T., Schneider, D.P., Strauss, M.A., & Kelly, B.C. 2007, ApJ, 656, 680

Kirkpatrick, A. et al. 2013, ApJ, 778, 51

Lacy, M. et al. 2004, ApJS, 154, 166

Laurent, O., Mirabel, I.F., Charmandaris, V., Gallais, P., Madden, S.C., Sauvage, M., Vigroux, L. & Cesarsky, C. 2000, A&A, 359, 887

Lonsdale, C.J. et al. 2003, PASP, 115, 897

Lu, N., Helou, G., Werner, M.W., Dinerstein, H.L., Dale, D.A., Silbermann, N.A., Malhotra, S., Beichman, C.A., & Jarrett, T.H. 2003 ApJ, 588, 199

Madden, S.C., Galliano, F., Jones, A.P., & Sauvage, M. 2006, A&A, 446, 877

Magdis, G.E. et al. 2013, A&A, 558, 136

Mendez, A.J. et al. 2013, ApJ, 770, 40

Mullaney, J.R., Alexander, D.M., Goulding, A.D., & Hickox, R.C. 2011, MNRAS, 414, 1082

Murphy, E.J, Chary, R.-R., Alexander, D.M., Dickinson, M., Magnelli, B., Morrison, G., Pope, A., & Teplitz, H.I. 2009, ApJ, 698, 1380

Murphy, E.J, Chary, R.-R., Dickinson, M., Pope, A., Frayer, D.T., & Lin, L. 2011, ApJ, 732, 126

Oliver, S.J. et al. 2010, A&A, 518, 21

Peeters, E., Spoon, H.W.W., & Tielens, A.G.G.M. 2004, ApJ, 613, 986

Petric, A.O. et al. 2011, ApJ, 730, 28

Popescu, C.C., Misiriotis, A., Kylafis, N.D., Tuffs, R.J., & Fischera, J. 2000, A&A, 362, 138

Richards, G.T. et al. 2006, ApJS, 166, 470

Rieke, G.H., Alonso-Herrero, A., Weiner, B.J., Pérez-González, P.G., Blaylock, M., Donley, J.L., & Marcillac, D. 2009, ApJ, 692, 556

Roussel, H. et al. 2006, ApJ, 646, 841

Shang, Z. et al. 2011 ApJS, 196, 2

Shi, Y., Helou, G., Armus, L., Stierwalt, S., & Dale, D.A. 2013, ApJ, 764, 28

Siebenmorgen, R. & Krügel, E. 2007, A&A, 461, 445

Silva, L., Granato, G.L., Bressan, A., & Danese, L. 1998, MNRAS, 337, 1309

Smith, J.D.T., et al. 2007, ApJ, 656, 770

Spoon, H.W.W., Marshall, J.A., Houck, J.R., Elitzer, M., Hao, L., Armus, L., Brandl, B.R., & Charmandaris, V. 2007, ApJ, 654, L49

Stierwalt, S. et al. 2013, ApJS, 206, 1

Stern, D. et al. 2005, ApJ, 631, 163

Wu, Y. et al. 2010, ApJ, 723, 895

Wu, Y. et al. 2011, ApJ, 734, 40

U, V. et al. 2012, ApJS, 203, 9

Yan, L. et al. 2013, AJ, 145, 55

Table 1. Coefficients for Determining 5-1100 μm Total Infrared Luminosity

AGN Fraction (%)	η_1	η_2	η_3	Max Error (%)	ζ_1	ζ_2	ζ_3	Max Error (%)	ξ_0	ξ_1	ξ_3	ξ_3	Max Error (%)
00	2.333	−0.196	1.566	+6.7	1.548	0.767	1.285	+0.2	−0.173	1.541	0.766	1.368	−0.03
05	2.339	−0.200	1.568	+6.5	1.555	0.765	1.299	+0.1	−0.049	1.554	0.764	1.323	+0.04
10	2.346	−0.203	1.571	+6.4	1.562	0.763	1.314	+0.1	+0.006	1.562	0.763	1.311	+0.02
15	2.353	−0.208	1.574	+6.2	1.569	0.761	1.330	−0.1	+0.152	1.572	0.762	1.248	+0.12
20	2.346	−0.203	1.572	+6.2	1.572	0.763	1.344	−0.1	+0.012	1.572	0.763	1.337	−0.01
25	2.359	−0.212	1.577	+5.9	1.578	0.762	1.362	−0.1	+0.061	1.578	0.763	1.326	+0.03
30	2.355	−0.209	1.577	+5.8	1.583	0.763	1.382	−0.1	+0.009	1.583	0.763	1.377	−0.05
35	2.363	−0.214	1.580	+5.6	1.594	0.760	1.407	−0.2	+0.201	1.589	0.762	1.275	+0.08
40	2.360	−0.213	1.581	+5.4	1.601	0.761	1.432	−0.2	+0.072	1.598	0.762	1.381	−0.06
45	2.351	−0.207	1.580	+5.3	1.612	0.759	1.464	−0.2	+0.200	1.601	0.762	1.315	+0.04
50	2.365	−0.216	1.584	+5.0	1.627	0.756	1.501	−0.3	+0.302	1.605	0.761	1.260	+0.08
55	2.367	−0.217	1.586	+4.7	1.642	0.755	1.542	−0.4	+0.281	1.615	0.760	1.300	+0.04
60	2.384	−0.227	1.589	+4.3	1.662	0.751	1.593	−0.5	+0.339	1.621	0.759	1.277	+0.03
65	2.381	−0.225	1.592	+4.0	1.680	0.751	1.653	−0.5	+0.363	1.625	0.760	1.281	+0.05
70	2.396	−0.234	1.592	+3.6	1.713	0.745	1.729	−0.6	+0.432	1.630	0.757	1.238	+0.05
75	2.384	−0.228	1.597	+3.3	1.743	0.744	1.825	−0.6	+0.454	1.633	0.759	1.243	+0.08
80	2.398	−0.236	1.596	+2.7	1.787	0.739	1.951	−0.7	+0.496	1.634	0.759	1.222	+0.07
85	2.403	−0.238	1.597	+2.2	1.852	0.730	2.123	−0.7	+0.515	1.645	0.756	1.233	+0.04
90	2.396	−0.236	1.613	+1.6	1.934	0.726	2.384	−0.6	+0.502	1.666	0.759	1.325	+0.01
95	2.412	−0.244	1.595	+0.9	2.081	0.708	2.789	−0.5	+0.561	1.662	0.757	1.262	+0.02

Note. — The coefficients pertain to Equations 3, 4, and 5, and the maximum errors refer to the largest deviations from the (noiseless) model total infrared luminosity over the range of $\alpha_{\rm SF}$.

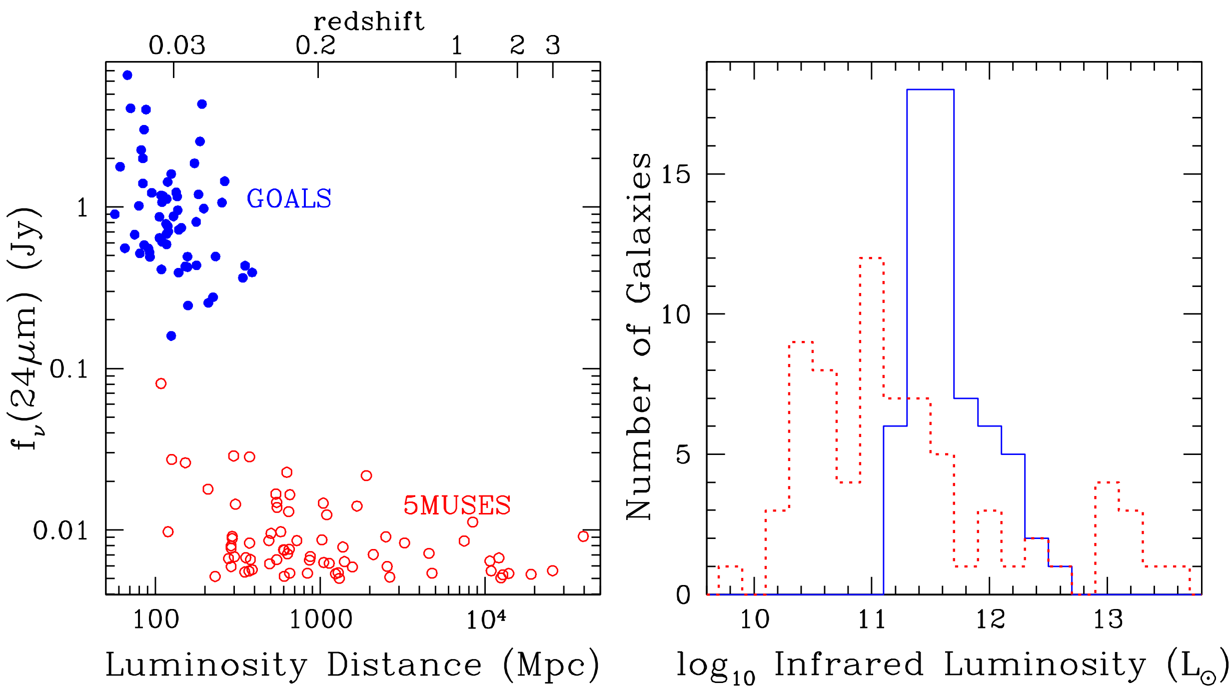

Fig. 1.— The (subsets of the) two comparison samples used in this work. The subset of the 5MUSES sample (Wu et al. 2010) is the 74 sytems with available *Spitzer* and *Herschel/SPIRE* photometry (Magdis et al. 2013) and the subset of the GOALS sample (Armus et al. 2009) is the 64 targets with *Spitzer* photometry (U et al. 2012). The luminosities in the righthand panel come from U et al. (2012) (GOALS) and this work (5MUSES).

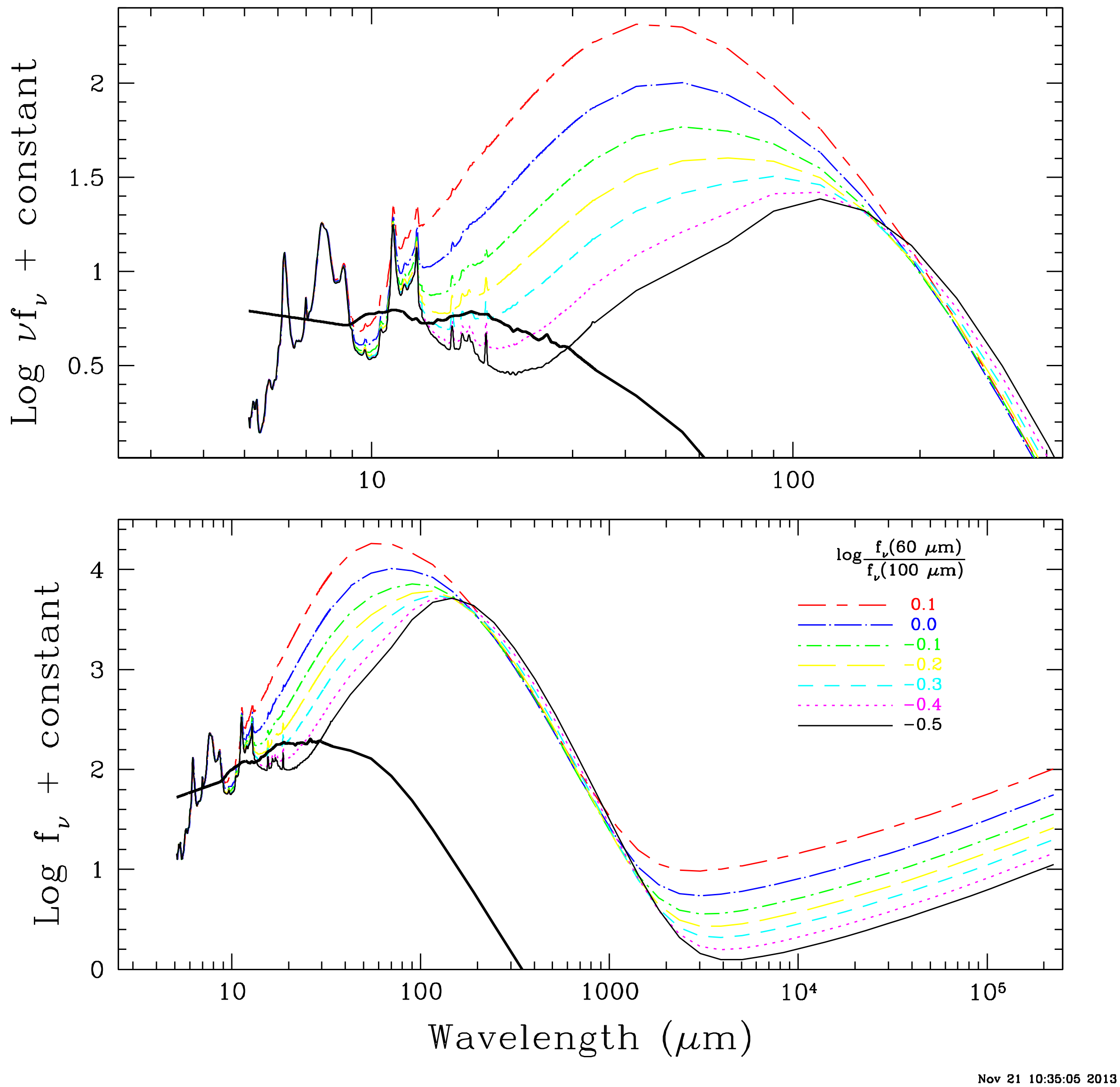

Fig. 2.— A collection of seven pure star-forming model spectral energy distributions along with that for a pure AGN. The star-forming spectra are essentially the suite of curves presented in Dale & Helou (2002), but with the ISOPHOT mid-infrared template replaced by the star-forming template of Spoon et al. (2007) (their "1C" curve). The different star-forming curves portrayed here represent different α_{SED} values. The AGN spectrum derives from the median radio-quiet quasar spectral energy distribution of Shang et al. (2011), but with a modification beyond ~120 μm (see § 3.2).

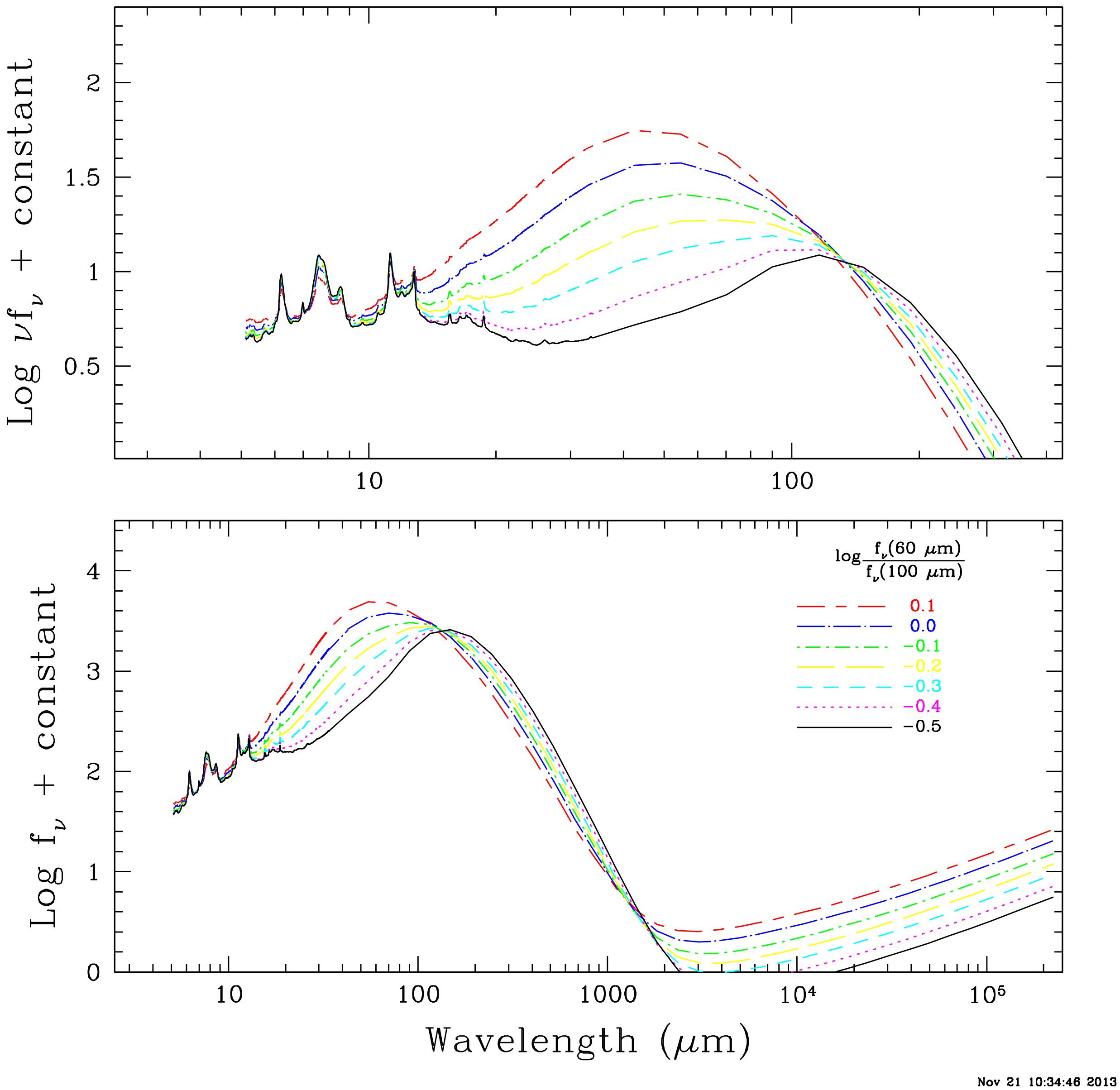

Fig. 3.— The model curves that result from equally combining the pure star-forming and radio-quiet quasar curves from Figure 2. "Equal" implies a 50% contribution to the emission over 5-20 μm.

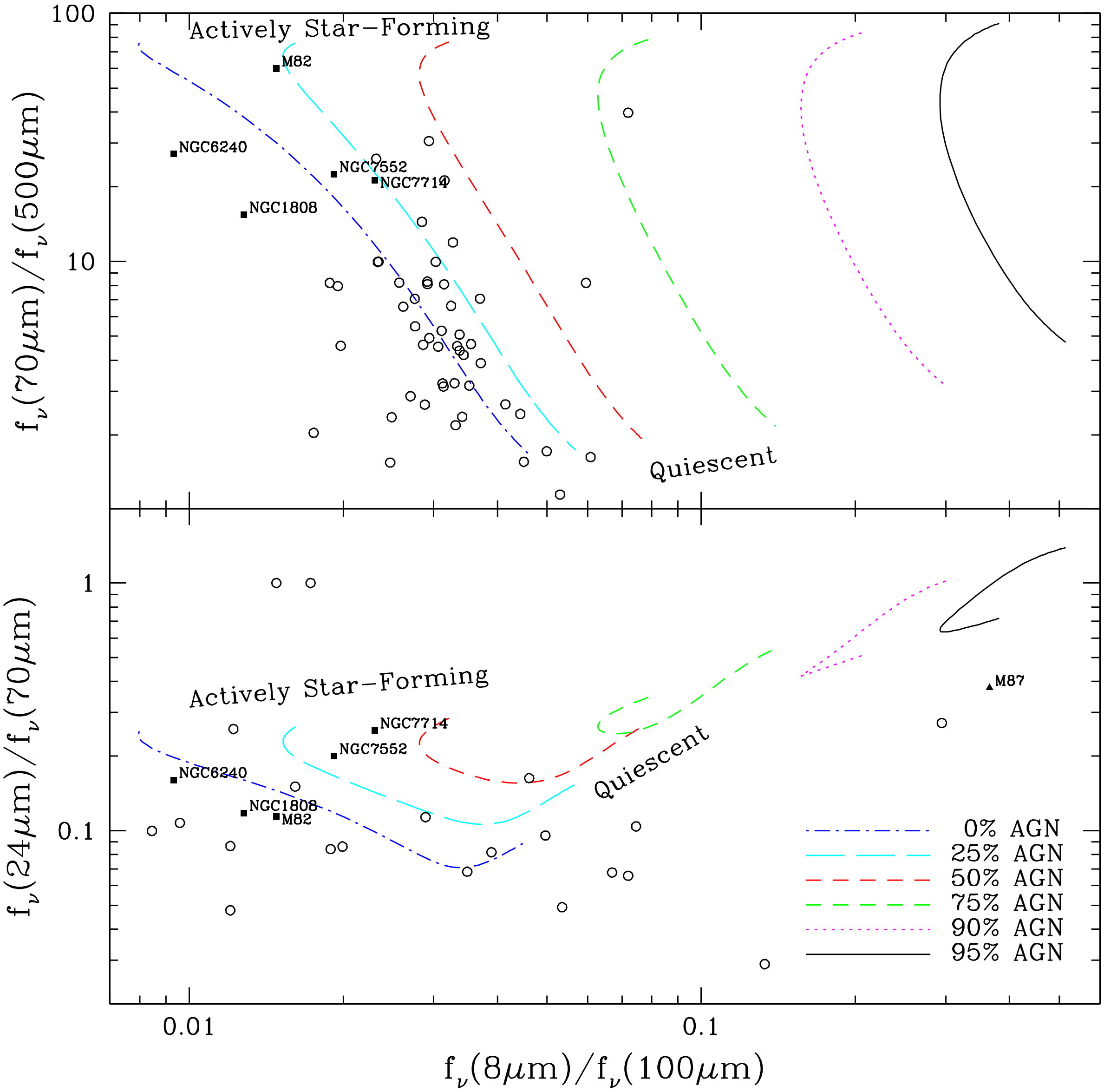

Fig. 4.— Rest-frame color-color diagrams for the joint AGN-star-forming spectral energy distribution models. The colors for actively star-forming galaxies (filled squares) come from Siebenmorgen & Krügel (2007), the colors for normal star-forming galaxies (open circles) are from Dale et al. (2012), and the colors for the local AGN M 87 (filled triangle) are from the NASA/IPAC Extragalactic Database. The range of model colors displayed for a given mid-infrared AGN percentage represents the diversity of colors in the star-forming templates; the color spread for a single AGN percentage indicates the impact of varying $\alpha_{\rm SF}$.

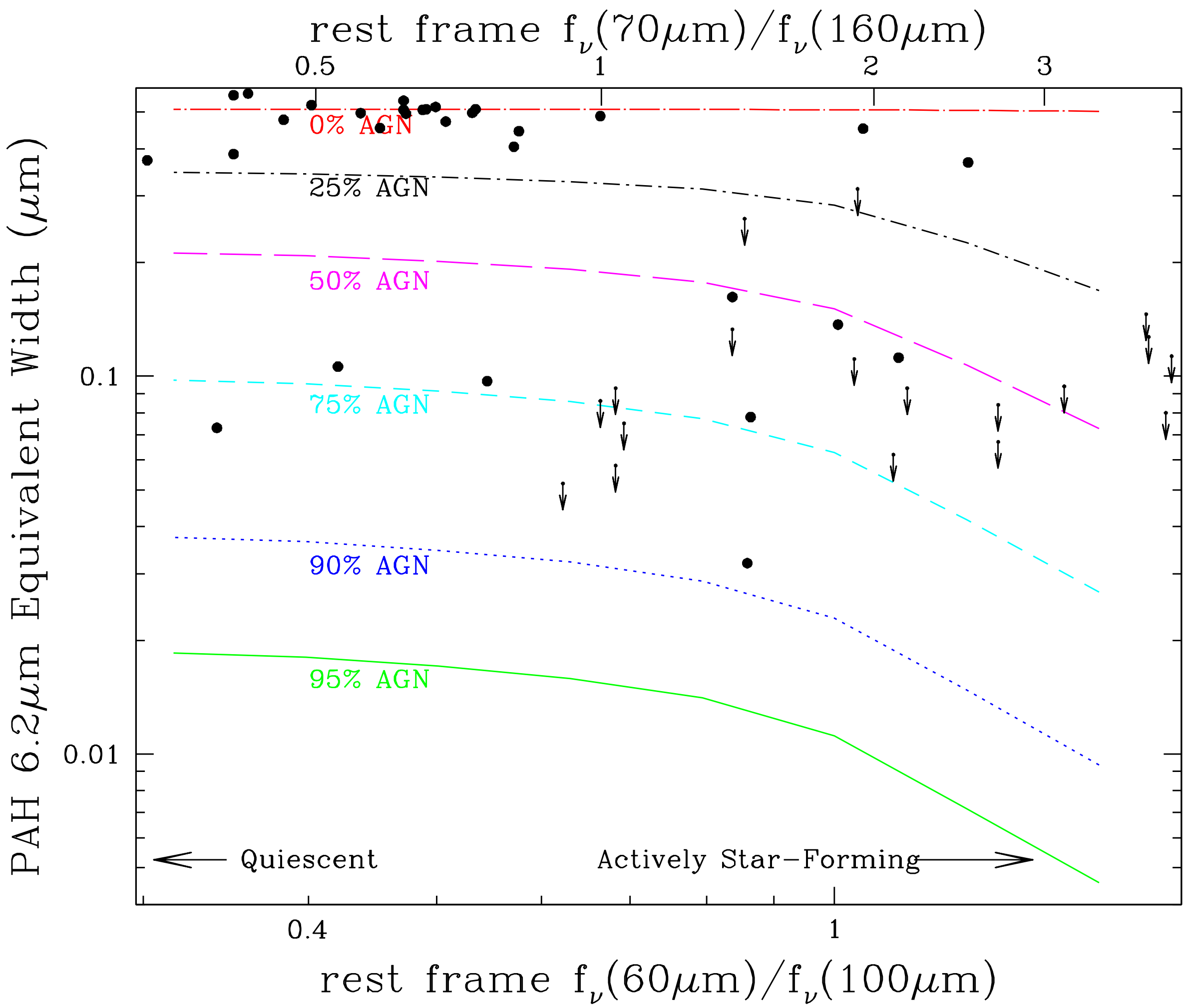

Fig. 5.— PAH 6.2 μm equivalent width as a function of far-infrared color. The different curves indicate the trends for varying mid-infrared fractional levels of AGN. The data points represent the 5MUSES survey; the colors are based on the fits shown in Figure 6.

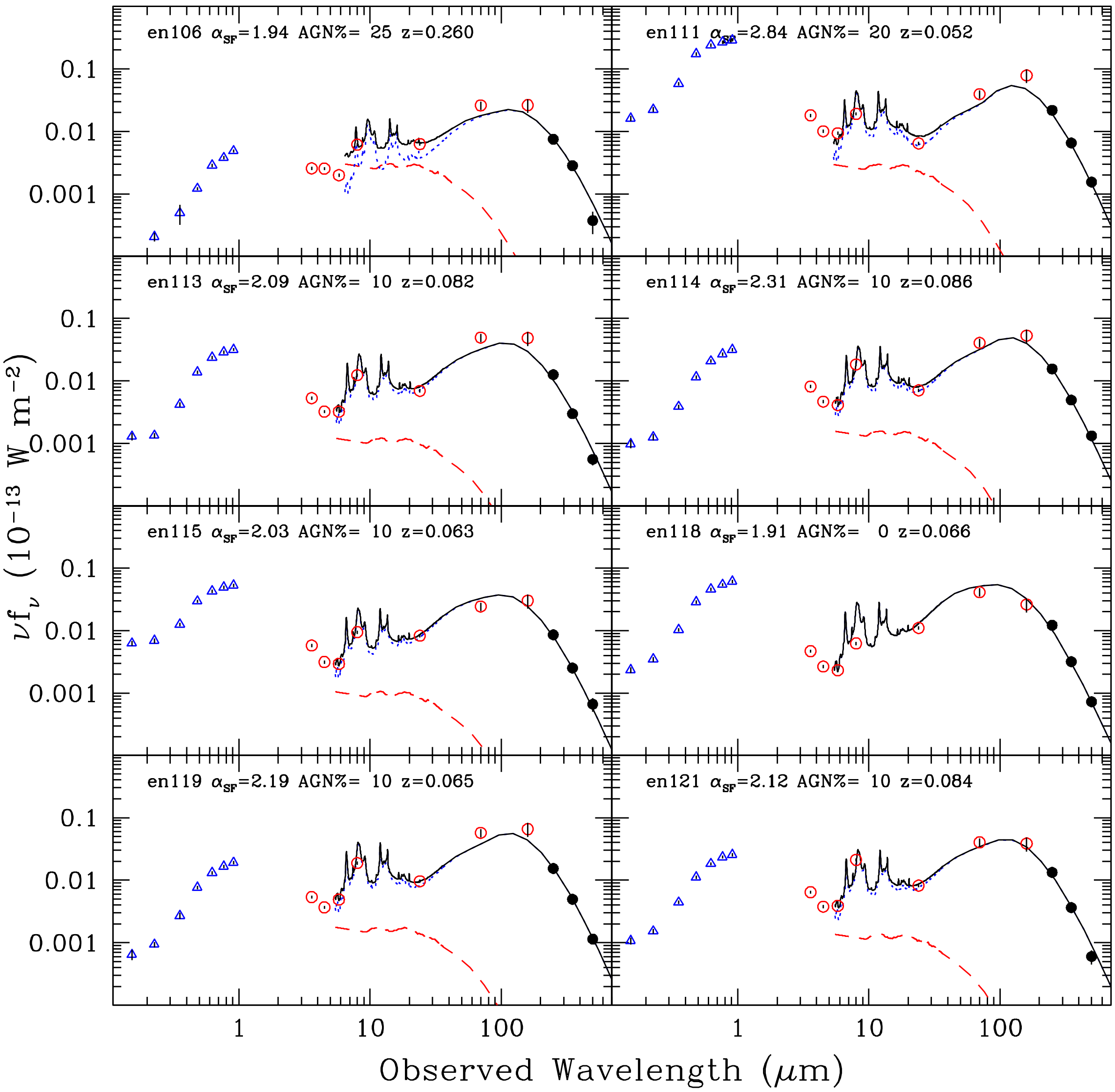

Fig. 6.— Globally-integrated infrared/sub-millimeter spectral energy distributions for the 5MUSES sample of 24 μm-selected galaxies (Wu et al. 2010; Magdis et al. 2013), sorted by Right Ascension. Open circles represent *Spitzer* data, filled circles are from the *Herschel Space Observatory*, and open triangles stem from *GALEX* and the Sloan Digital Sky Survey. The blue dotted and red dashed lines respectively trace the star-forming and AGN components.

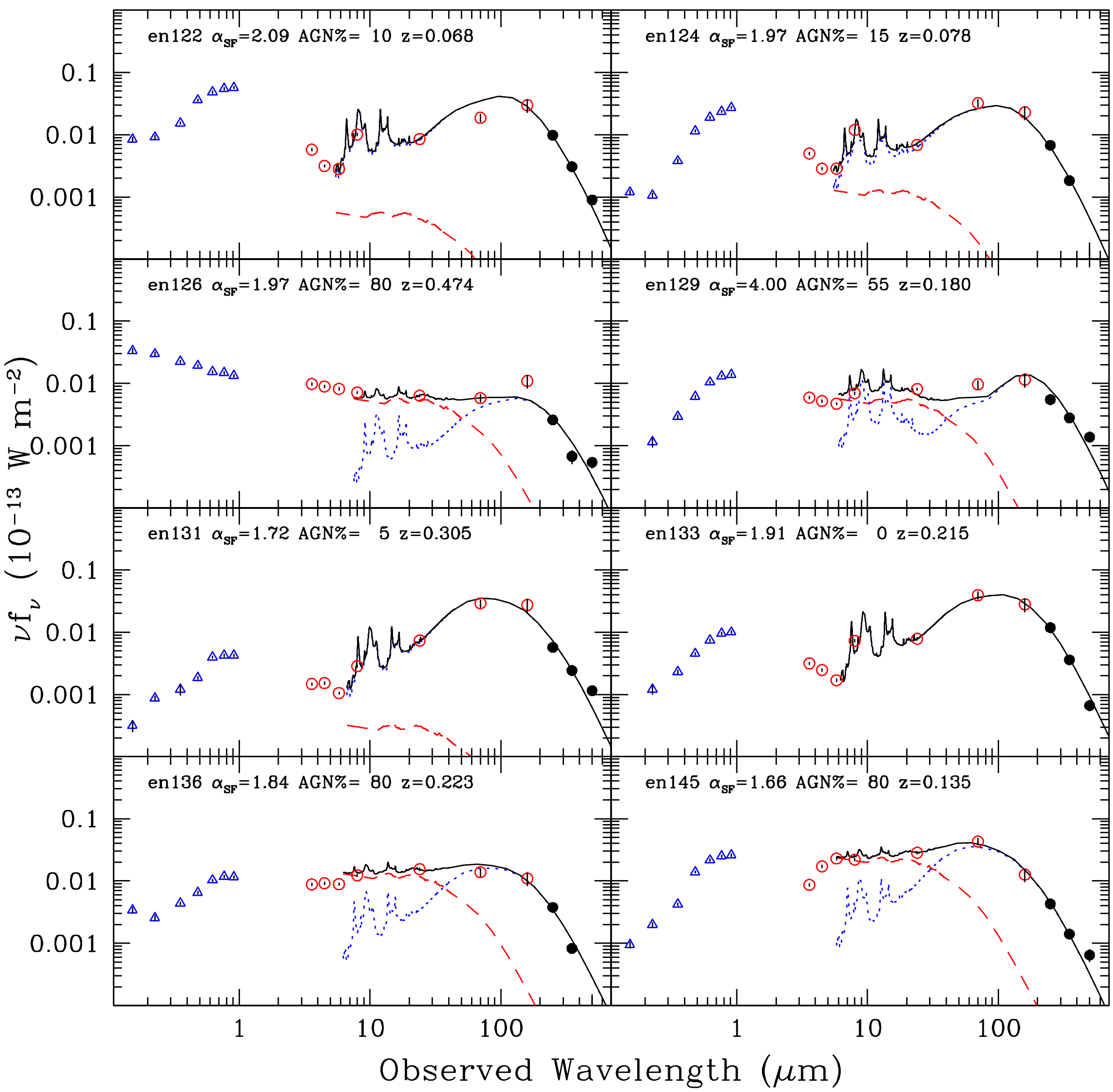

Fig. 6.— (Continued)

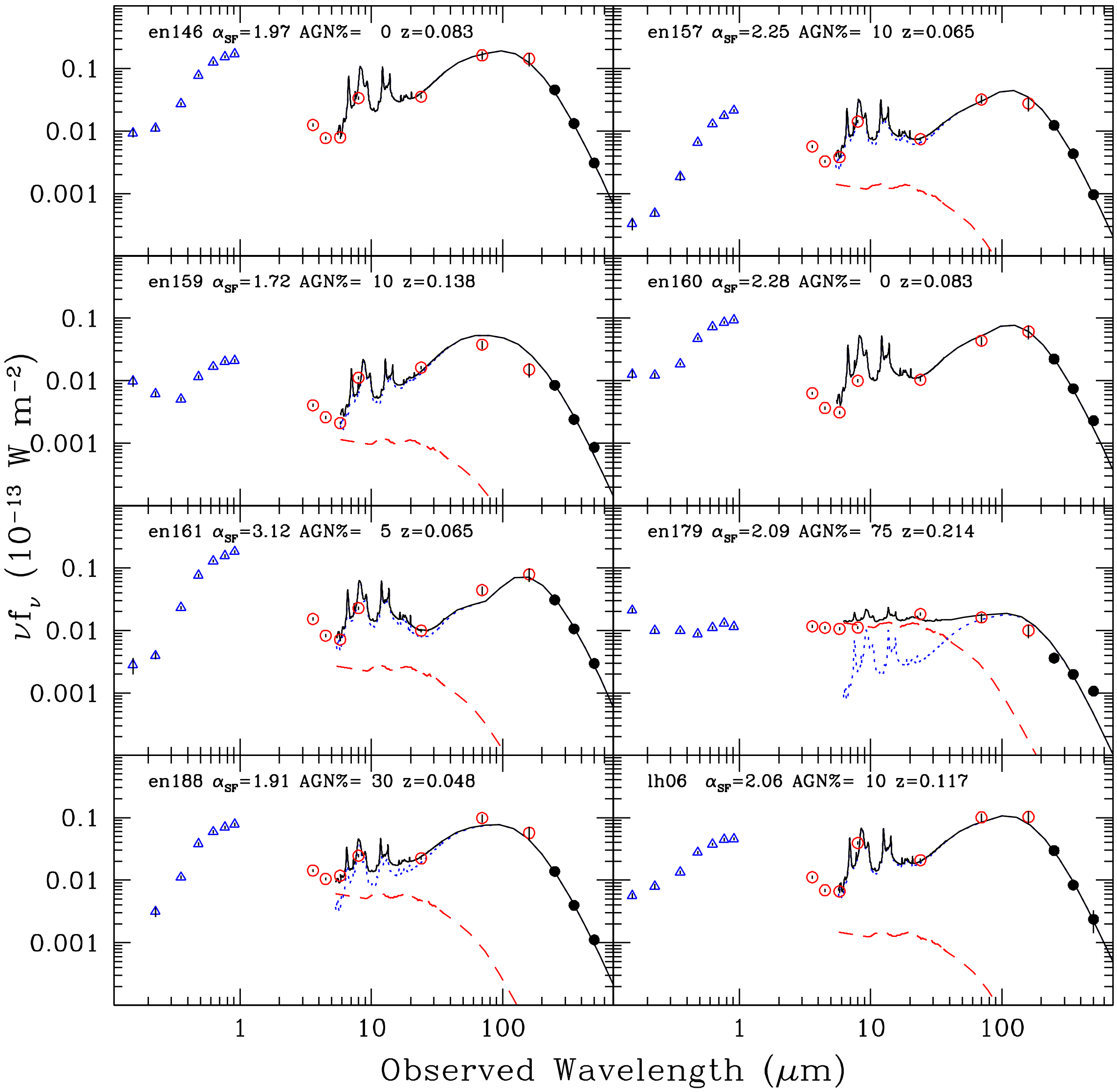

Fig. 6.— (Continued)

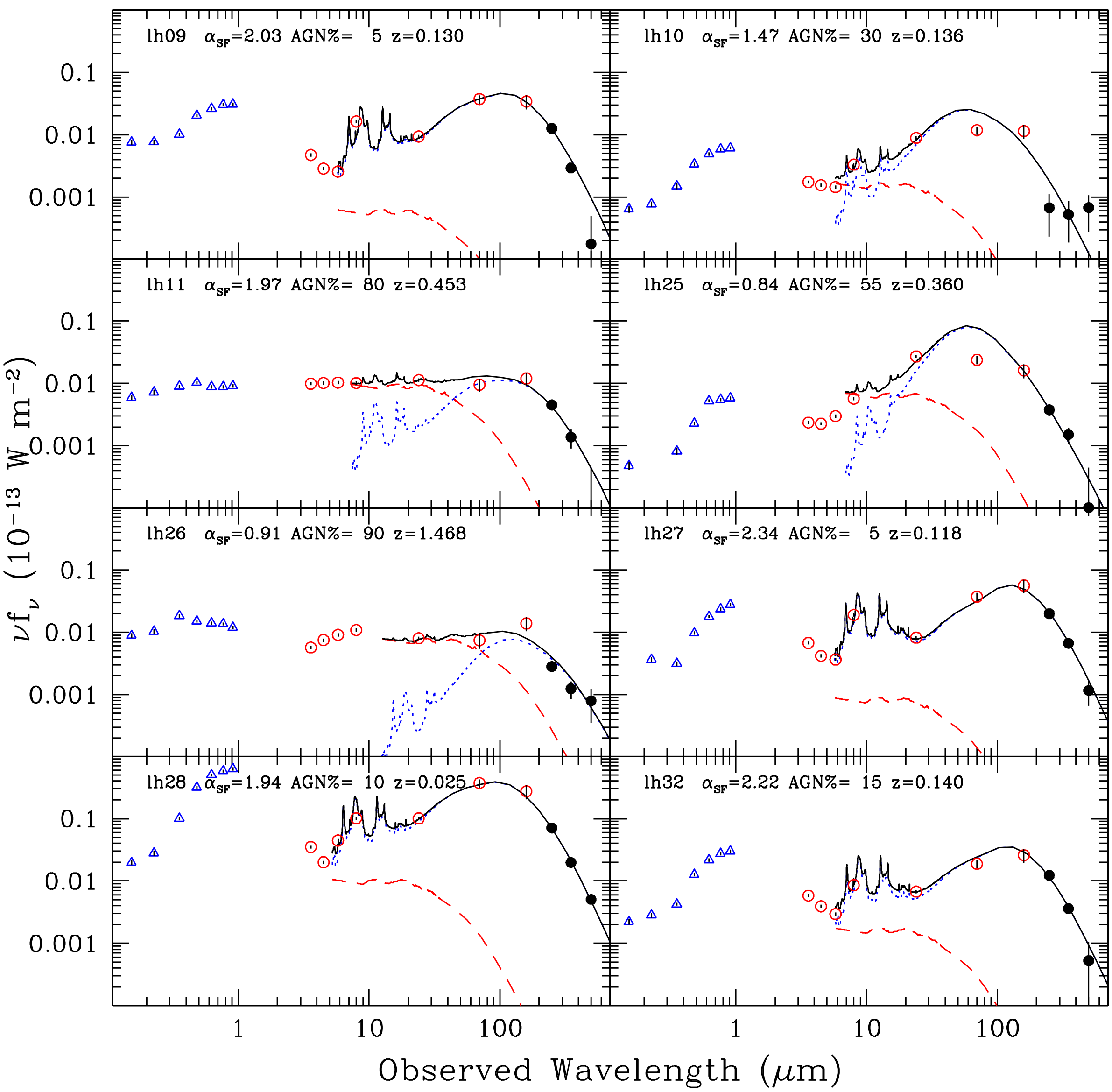

Fig. 6.— (Continued)

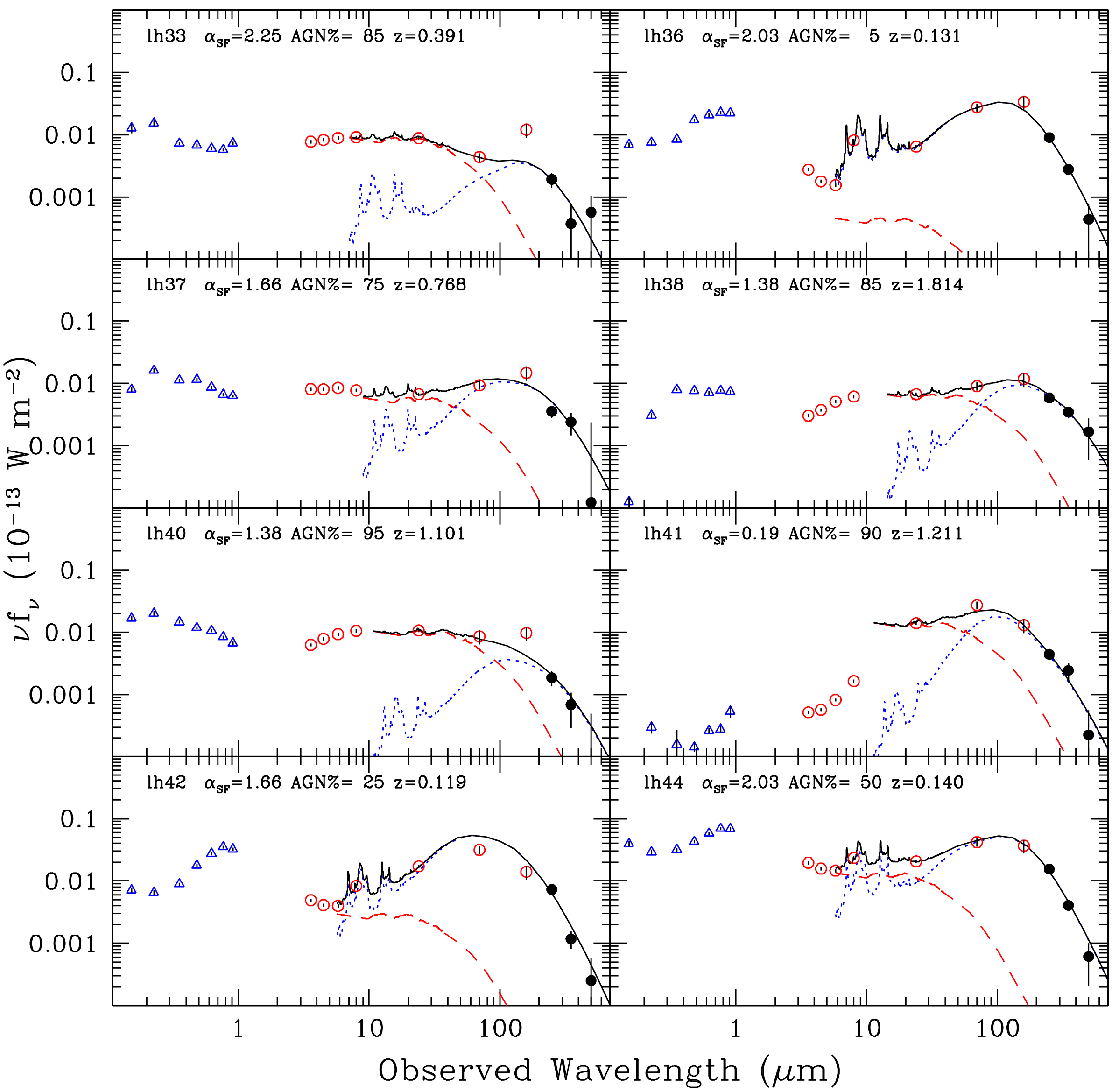

Fig. 6.— (Continued)

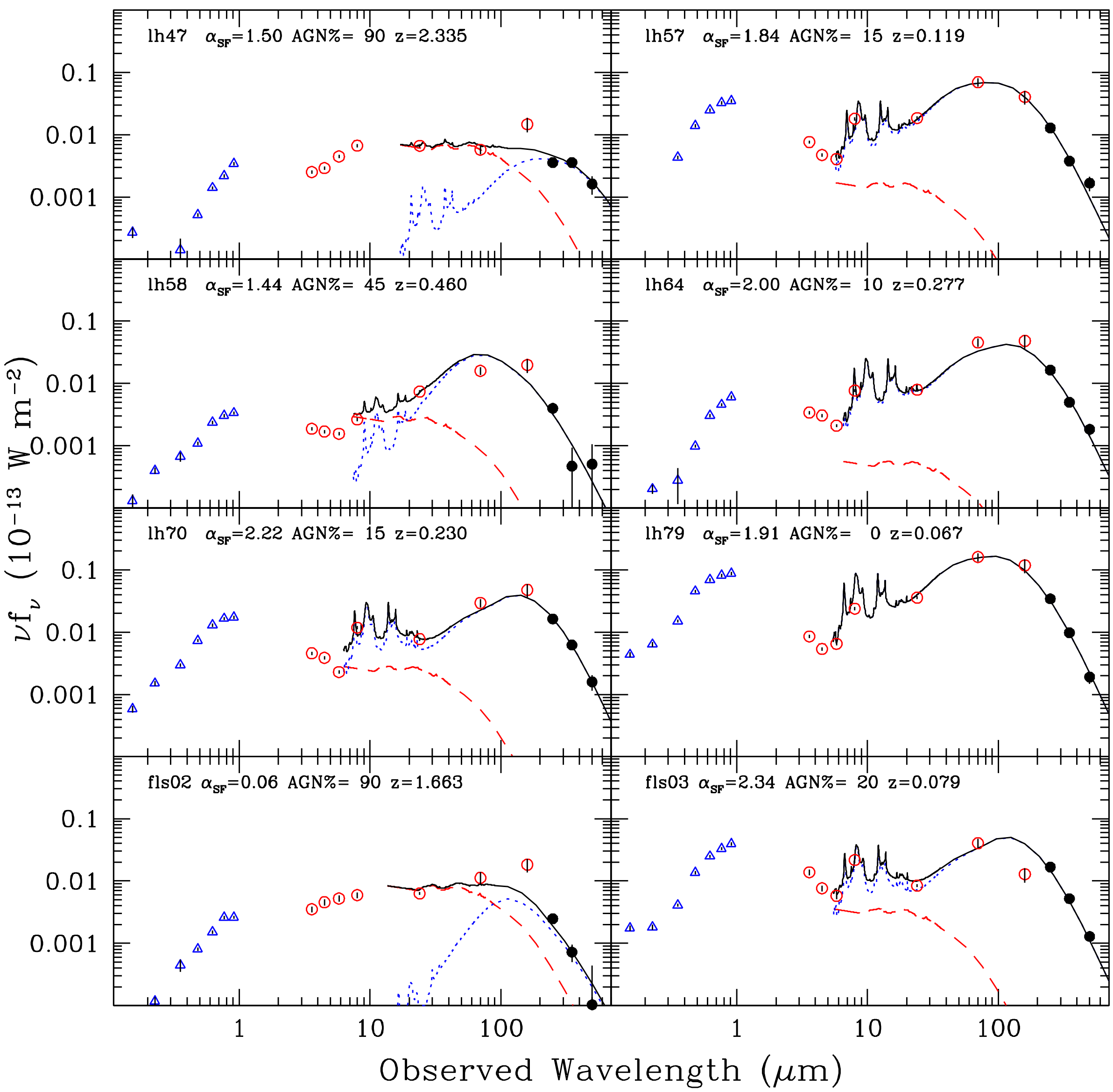

Fig. 6.— (Continued)

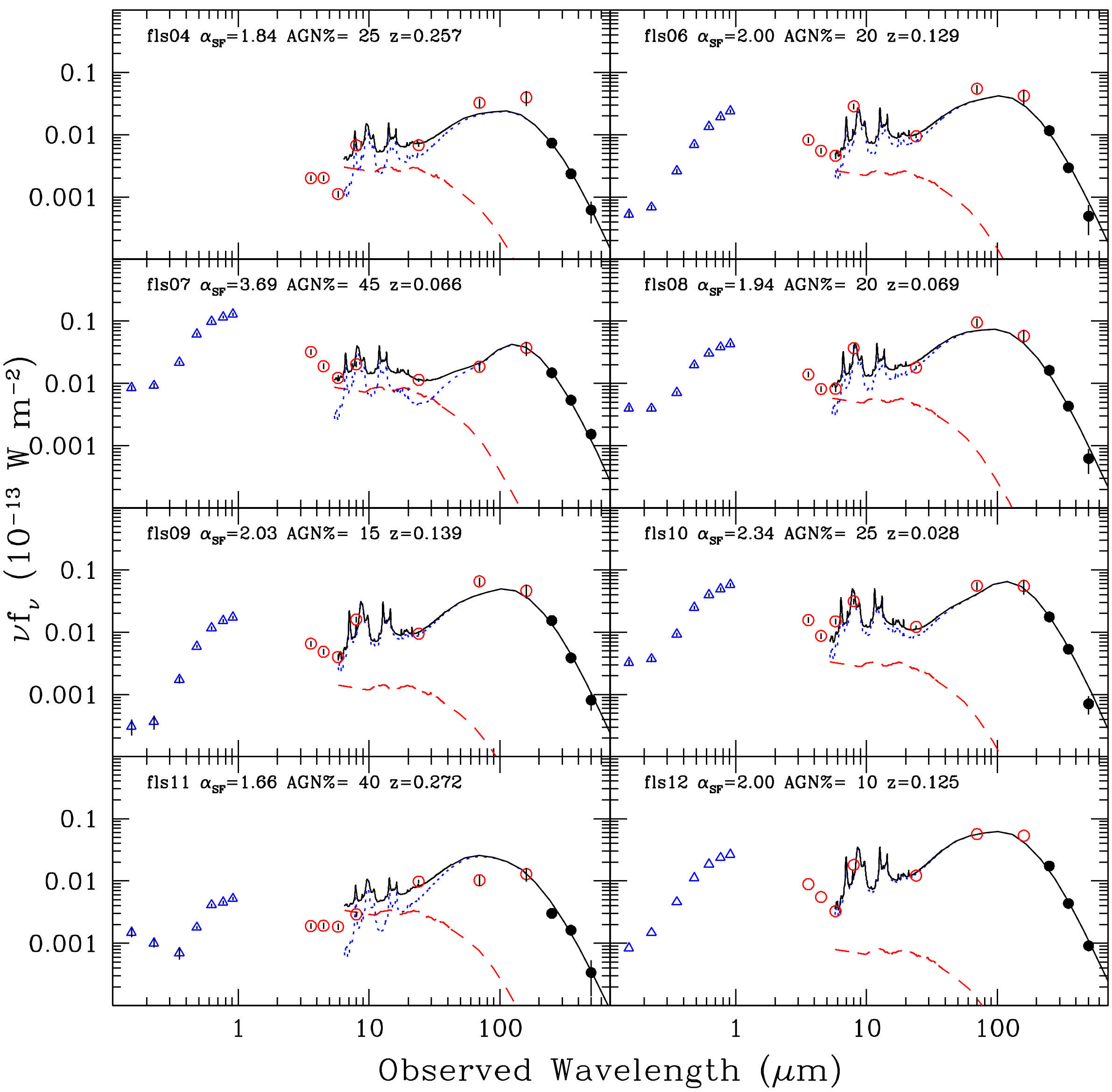

Fig. 6.— (Continued)

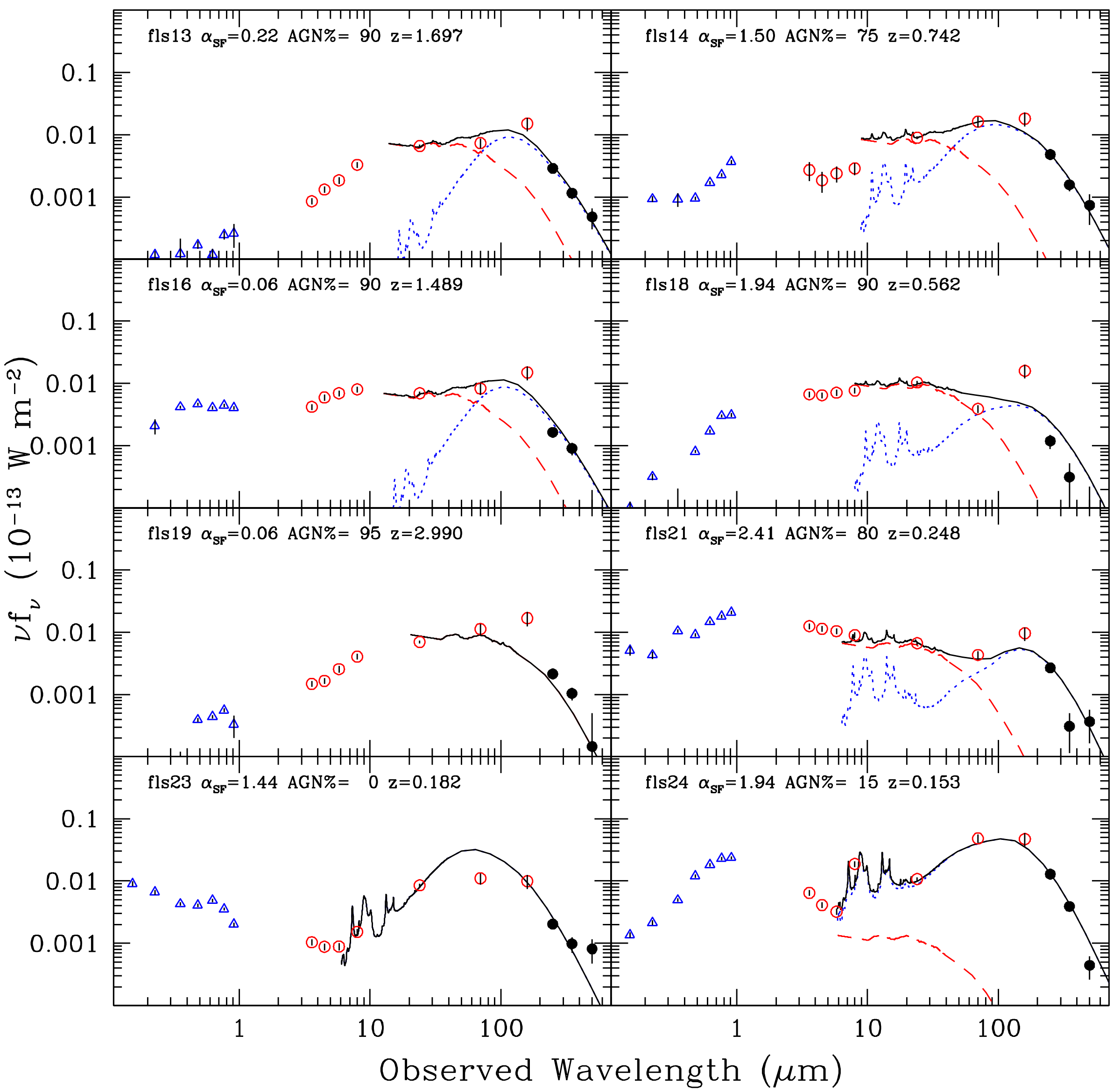

Fig. 6.— (Continued)

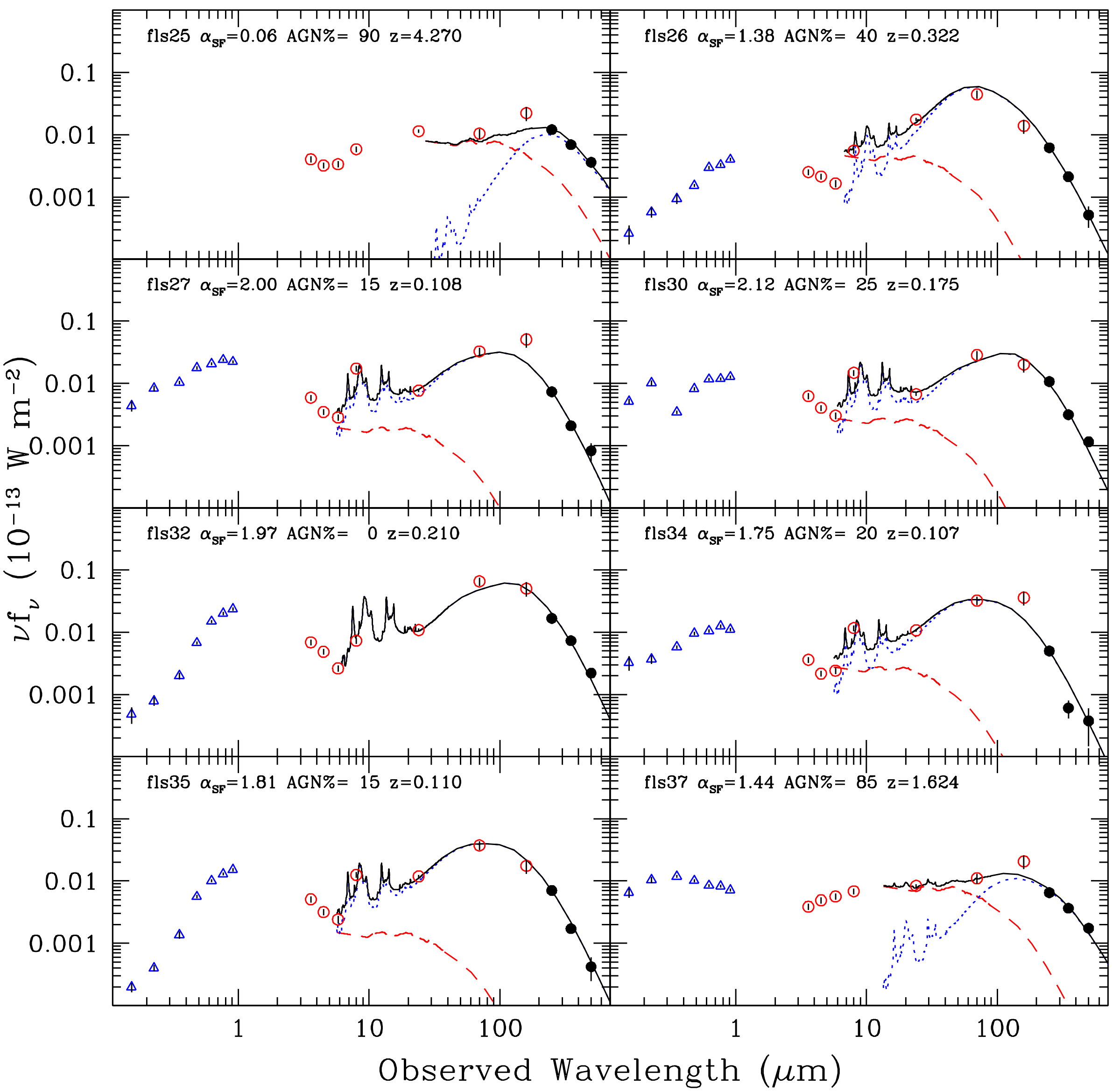

Fig. 6.— (Continued)

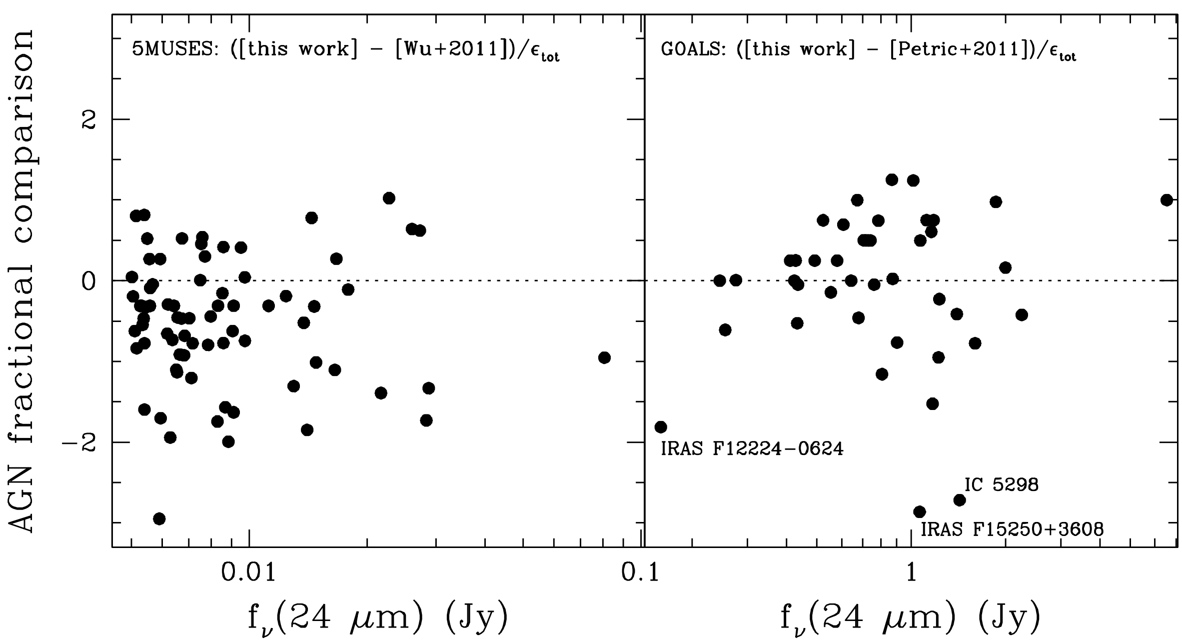

Fig. 7.— Comparison of mid-infrared AGN fractional estimates in the literature to those from our 5.8–160 μm broadband SED-fitting approach. The mid-infrared AGN fractional differences are normalized by the total uncertainty, which is a sum in quadrature of the standard deviations in the Monte Carlo simulations decribed in § 4.4 along with an assumed 25% uncertainty for the literature values. *Left:* Compared to the 5–35 μm continuum analysis of Wu et al. (2011). *Right:* Compared to the PAH(6.2 μm) + 6–15 μm continuum analysis of Petric et al. (2011).

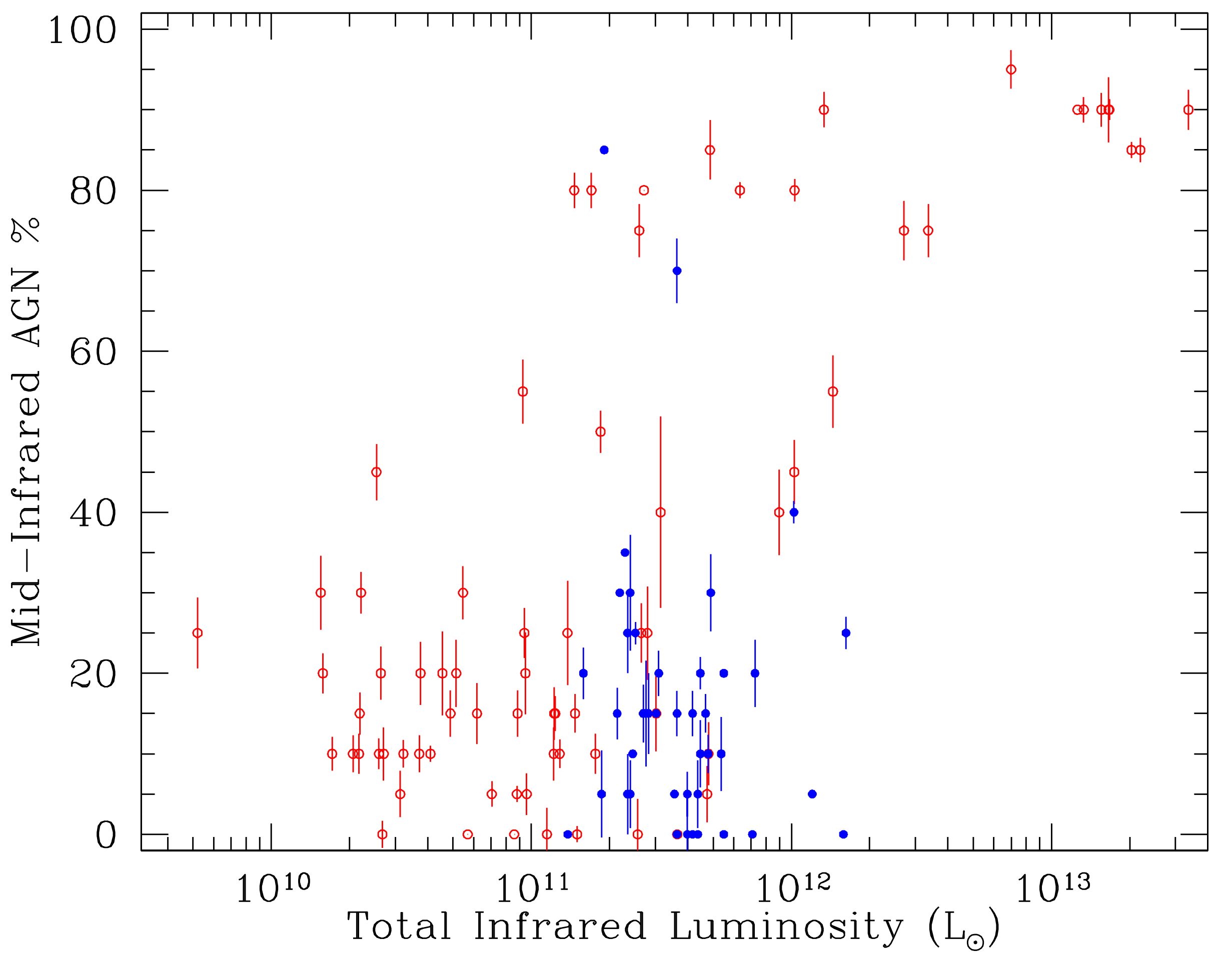

Fig. 8.— Our template-based 5MUSES (open red circles) and GOALS (filled blue circles) AGN mid-infrared fractions as a function of infrared luminosity.